17th World Conference on Earthquake Engineering, 17WCEE
Sendai, Japan - September 13th to 18th 2020

SEISMIC PERFORMANCE OF SUSPENDED PIPING RESTRAINT INSTALLATIONS

D. Perrone[(1)], A. Filiatrault[(2)], S. Peloso[(3)], E. Brunesi[(4)], R. Nascimbene[(5)], C. Beiter[(6)], R. Piccinin[(7)]

[(1)] *Postdoctoral Researcher, University School for Advanced Studies IUSS Pavia, Pavia, Italy, daniele.perrone@iusspavia.it*
[(2)] *Professor, Department of Civil, Structural and Environmental Engineering, State University of New York at Buffalo, Buffalo, USA & University School for Advanced Studies IUSS Pavia, Pavia, Italy, af36@buffalo.edu*
[(3)] *Researcher, European Centre for Training and Research in Earthquake Engineering, Pavia, Italy, simone.peloso@eucentre.it*
[(4)] *Researcher, European Centre for Training and Research in Earthquake Engineering, Pavia, Italy, emanuele.brunesi@eucentre.it*
[(5)] *Researcher, European Centre for Training and Research in Earthquake Engineering, Pavia, Italy, roberto.nascimbene@eucentre.it*
[(6)] *Researcher, Hilti Corporation, Schaan, Liechtenstein, Clemens.Beiter@hilti.com*
[(7)] *Researcher, Hilti Corporation, Schaan, Liechtenstein, Roberto.Piccinin@hilti.com*

Abstract

The damage observed during past earthquakes repeatedly showed the vulnerability of non-structural elements and their importance in the functionality of critical facilities, such as hospitals. Performance-based seismic design (PBSD) implies the harmonization of performances between structural and non-structural elements. To this aim, performance parameters for non-structural elements need to be evaluated through experimental and numerical studies. Among the multitude of non-structural typologies, the seismic performance of piping systems is of paramount importance in order to guarantee the immediate post-event functionality of critical facilities. Few research studies available in the literature have attempted to evaluate the performance parameters required to enable PBSD of piping systems and more specifically of suspended piping restraint installations. This paper summarizes the results of an experimental and numerical research project dealing with the evaluation of the seismic behaviour of suspended piping restraint installations. Four typologies of suspended trapeze piping restraint subassemblies with channel and rod bracing systems were tested under monotonic and cyclic loading to determine their hysteretic responses and failure modes. The results of the subassembly tests were used to calibrate simplified nonlinear numerical models useful to assess the seismic response of full-scale suspended piping layouts subjected to floor acceleration time-histories.

Keywords: Non-structural elements, suspended piping restraint installations, piping, experimental testing, numerical modelling.

1. Introduction

The reconnaissance carried out following recent earthquakes repeatedly demonstrated the importance of non-structural elements in the loss estimation framework as well as in the functionality of critical facilities [1-5]. It is nowadays recognized that the performance of non-structural elements represent a key issue in the performance-based seismic design (PBSD) of new buildings and the retrofit of existing ones. The influence of non-structural elements in the PBSD can be summarized by two main issues: 1) non-structural elements generally exhibit damage at low seismic intensities with respect to supporting structures and 2) non-structural elements represent most of the total investments in typical buildings [6].

Following the 2010 Chile earthquake, the Santiago International Airport was closed for several days because of the severe damage to piping systems interacting with ceiling systems [5]. Similar inadequate performance of piping systems was also observed following the 2006 Hawaii Earthquake [4]. Analysing the damage to suspended piping systems, it can be stated that the weakest elements are the piping joints, which experience excessive rotations due to the inadequate bracing of the pipes, and the piping restraint installations [7,8]. The poor seismic performance of piping systems, and in general of non-structural elements, can be associated to two main factors: 1) few experimental data are available in the literature to assess their dynamic response and to define performance objectives to be achieved in the PBSD and 2) the design methodologies available in seismic codes and guidelines are generally empirical in nature and do not provide specific quantitative indications on how to achieve defined performance objectives within the PBSD framework.

A PBSD methodology for non-structural elements has been recently developed by Filiatrault *et al.* [9]. This methodology requires the definition of performance objectives for each damage limit state and the calibration of meaningful performance parameters characterizing the seismic response of non-structural elements. Focusing on suspended piping systems, two damage limit states can be considered in the PBSD: the serviceability limit state and the ultimate limit state. The attainment of the serviceability limit state can be related to the yielding of the trapeze restraint installations as well as to the leakage of the piping joints. Following this consideration, the displacement at which the yielding of the suspended piping restraint installations occurs and the piping joint leakage rotations should be quantified. The ultimate limit state of suspended piping systems can be related to visible distortion or failure of components associated with measurable drop in load bearing capacity.

A reliable quantification of non-structural elements performance parameters for use in PBSD involves the development of detailed system design information by means of quasi-static cyclic tests and/or numerical analyses. The cyclic tests and the numerical analyses should be performed both at the component and system levels. Focusing on piping systems, quasi-static cyclic tests can provide data to define meaningful performance parameters of suspended piping trapeze restraint installations and piping joints, such as the initial stiffness, the yield and maximum strengths, the ultimate deformation and the displacement ductility capacity.

The characterization of the dynamic response of piping joints has been recently investigated both from experimental and numerical point of views [7,8,10,11]. These recent studies mainly concerned the response of piping joints used in sprinkler piping systems and medical gas lines. In terms of cyclic response of suspended piping trapeze restraint installations, few studies are available in the literature [12,13].

This paper summarizes the results of an experimental and numerical research project dealing with the evaluation of the cyclic response of suspended piping restraint installations. Four typologies of suspended trapeze piping restraint subassemblies with channel and rod bracing systems were tested under monotonic and cyclic loading to determine their hysteretic responses and failure modes. The results of the subassembly tests were used to calibrate simplified nonlinear numerical models useful to assess the seismic response of full-scale suspended piping layouts subjected to floor acceleration time-histories.

2. Definition of trapeze restraint installations

The improvement of the seismic performance of suspended piping systems can be achieved through various typologies of sway bracing systems in order to provide lateral restraints to the pipes. Seismic restraint installations are mainly used in critical facilities and industrial buildings due to the large number of piping systems, equipment and non-structural elements required for their continuous functionalities. The results of a field survey carried out in Italian industrial and commercial facilities indicated that the most used seismic restraint installations are ceiling applications made of channel frames and rod trapezes. Based on this information, four suspended trapeze restraint installations were selected for this study (Figure 1).

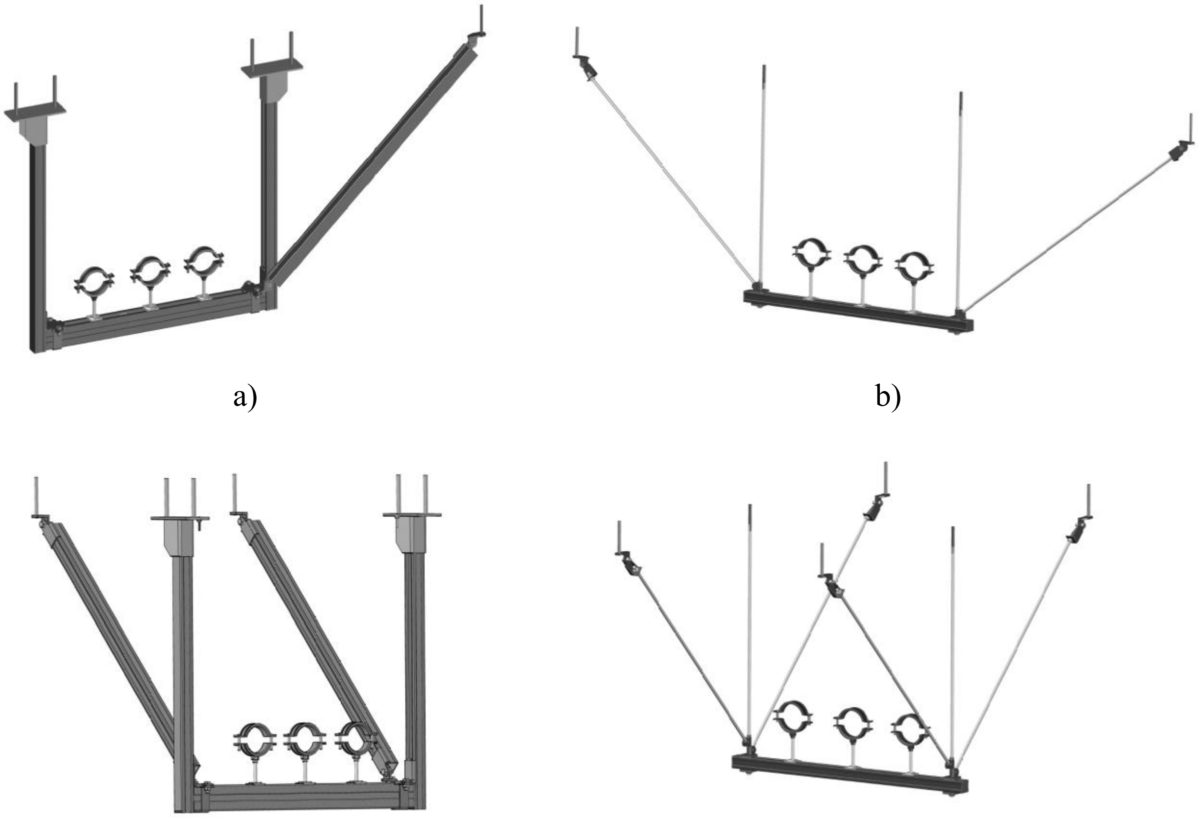

a) b) c) d)

Fig. 1 - Suspended trapeze restraint installations: a) Trapeze with transverse channel bracing system (SS1), b) Trapeze with transverse rod bracing system (SS2), c) Trapeze with longitudinal channel bracing system (SS3), d) Trapeze with transverse rod bracing system (SS4).

The first two seismic trapeze restraint installations consist of channel (Figure 1a) and rod (Figure 1b) trapezes braced in the transverse direction with respect to the pipes' direction. The channel and rod trapeze installations braced in the transverse direction are referred herein respectively as "SS1" and "SS2". These two configurations typically include two vertical channels/rods connected by a horizontal channel. In the case of the channel configuration, one diagonal element is used to provide lateral restraint, while for the rod trapeze two diagonal rods are installed to provide the lateral restraint. The channels' size is commonly equal to 41 mm square, while the rods' diameter is generally equal to 10 mm. The third and fourth typologies, referred herein as "SS3" and "SS4", consist of channel (Figure 1c) and rod (Figure 1d) trapeze assemblies with longitudinal bracing elements. Configuration "SS3" includes two diagonal channels inclined at an angle of 45° from the vertical to provide the longitudinal lateral bracing. Similar considerations in terms of inclination apply to configuration "SS4", but in this case four diagonal bracing rods are used. The connections between the steel channels and the threaded rods are guaranteed by hinges, while the connections between the vertical and diagonal elements and the supporting structure are provided by rail supports for the channel trapeze installations and by hinges for the rod trapeze installations. Finally for all typologies, short threaded rods are connected to the horizontal channel through steel plates in order to connect the pipes to the trapeze installations. The pipes are secured in place by means of pipe rings bolted to the threaded rods. Table 1 summarizes the main geometrical properties of the four suspended restraint trapeze installations considered in this study.

Table 1 - Main geometrical properties of suspended piping trapeze installations.

ID	Frame Typology	Bracing Direction	Brace Inclination (°)	Number of Braces	Horizontal Channel Length (mm)	Height of Vertical Channels or Rods (mm)
SS1	Channel	Transverse	45°	1	800	800
SS2	Rod	Transverse	45°	2	900	600
SS3	Channel	Longitudinal	45°	2	800	800
SS4	Rod	Longitudinal	45°	4	900	600

3. Sub-assembly testing

In order to investigate the global response of the selected suspended piping restrain trapeze installations, a specific experimental set-up was designed and realized. The experimental set-up consisted of a 3 m high steel frame connected to the strong floor of the laboratory through a system of steel beams and post-tensioned bars. The steel frame was designed to have a stiffness of at least two orders of magnitude greater than the specimens' stiffness. Figure 2 shows photographs of the experimental set-up. For each test, two trapeze installations were suspended simultaneously to a system of steel plates that simulated the supporting building's floor. The two specimens, spaced one meter apart, were connected to each other by four rigid pipes. The pipes were kept in place using four stiff pipe rings, which were connected to the horizontal channel of the trapeze installations through short threaded rods with a diameter equal to 12 mm. A gravity weight of 1.5 kN was applied in each test to simulate a typical configuration of four steel pipes supported by adjacent trapeze installations spaced 3 m apart [14]. Because the length of the pipes was shorter than 3 meters, an additional mass was placed at mid-length of the pipes. The horizontal load was applied through a horizontal actuator connected to a reaction wall and to the steel pipes. An array of potentiometers was used to measure displacements at key locations on the test specimens [13].

a) b)

Fig. 2 - a) Photograph of experimental set-up and b) Close-up of SS3 test specimen.

The experimental program consisted of 12 tests; four monotonic and eight cyclic tests were carried out (Table 2). All specimens were tested in their braced directions. For each configuration, one monotonic and two cyclic tests were performed. The monotonic tests were used to calibrate the corresponding cyclic loading protocol. The monotonic loading protocol consisted of a linear ramp until the maximum actuator displacement limit or the failure of the specimen occurred. Failure of a test specimen was defined when a 20% decay of the maximum horizontal load was observed. A slow loading rate was set equal to 0.5 mm/s for each monotonic test in order to avoid inertia effects. The cyclic tests were carried out following the FEMA 461 quasi-static cyclic loading protocol [15]. This cyclic loading protocol includes two cycles at each displacement amplitude. Table 2 lists all the parameters required to reproduce the quasi-static cyclic loading protocol used for each configuration. In this table, Δ_o is the target smallest deformation amplitude of the loading history and Δ_m represents the target maximum deformation amplitude of the loading history obtained from a preliminary monotonic test. To reach the target maximum deformation, Δ_m, 10 amplitudes were used.

Table 2 – Description of the experimental program.

Test ID	Configuration	Brace Direction	Load Direction	Monotonic Test	Cyclic Test	Δ_o (mm)	Δ_m (mm)
1	SS1	Transversal	Transversal	X			
2	SS1	Transversal	Transversal		X	1.0	21.3
3	SS1	Transversal	Transversal		X	1.0	21.3
4	SS2	Transversal	Transversal	X			
5	SS2	Transversal	Transversal		X	1.3	27.0
6	SS2	Transversal	Transversal		X	1.3	27.0
7	SS3	Longitudinal	Longitudinal	X			
8	SS3	Longitudinal	Longitudinal		X	1.7	36.0
9	SS3	Longitudinal	Longitudinal		X	1.7	36.0
10	SS4	Longitudinal	Longitudinal	X			
11	SS4	Longitudinal	Longitudinal		X	4.5	91.9
12	SS4	Longitudinal	Longitudinal		X	4.5	91.9

The results of the monotonic tests, in terms of load-displacement response, are plotted in black solid lines in Figure 3. The channel specimen SS1 achieved a maximum load equal to 14.1 kN, corresponding to a displacement of 19 mm (Figure 3a). Increasing the displacement caused the load immediately dropped to 10 kN at a displacement equal to 21 mm due to the yielding of the hinge connecting the diagonal and vertical channels. This yielding of the channel hinge caused differential translations between the two trapezes and a significant rotation of the specimen up to the end of the test. A lower capacity was recorded for Specimen SS2, which was also braced in the transverse direction of the pipes but was composed of rod elements. In particular, the maximum load recorded during the monotonic test was equal to 12.5 kN, corresponding to a displacement of 14 mm (Figure 3c). The load dropped to 8 kN at the maximum displacement (more than 75 mm). It was observed during the test that the braced started buckling at a displacement equal to 40 mm. Different deformations of the braces were observed in the two trapezes during the tests. In one trapeze, the diagonal rods buckled in plane while in the other one the diagonal rods buckled out-of-plane. These different behaviours caused a signification rotation of Specimen SS2, increasing further the displacements of the specimen. Although significant deformations of the specimen were reported at the end of the test, no failure of the components was observed. During the monotonic tests a higher horizontal capacity was recorded for the two specimens braced in the longitudinal direction. The longitudinal channel trapeze installation SS3 achieved a maximum capacity equal to 19.1 kN corresponding to a displacement equal to 39 mm (Figure 3e). Significant deformations of the threaded rods connection the pipes to the horizontal channel were observed. These deformations induced torsional deformations in the horizontal channel in one of the two trapezes. In the other trapeze, the horizontal channel moved downwards due to the sliding of the component connecting the vertical and horizontal channel. Due to the different deformations of the two trapezes, the specimen experienced a significant rotation. The test was stopped at a displacement equal to 80 mm due to the failure of one of the threaded rods connecting the pipe-ring to the horizontal channel. The last monotonic test was conducted on the SS4 configuration, which was braced also in the longitudinal direction but was composed of rod elements. The maximum load achieved during the test was equal to 22.2 kN, corresponding to a displacement of 37 mm (Figure 3g). Similar to Specimen SS2, significant deformations of the diagonal and vertical rods were observed, thereby increasing the displacement of the specimen from a displacement equal to 25 mm. A flexural-torsional yielding of the horizontal channels was reported during the test; the associated deformations also caused inelastic deformations in the short threaded rods connecting the pipe-rings to the horizontal channels. Although no failure was observed, the test was stopped at a displacement equal to 60 mm when the applied load dropped beyond 20% of its maximum value.

For each configuration, two cyclic tests were also performed. Figures 3a to 3h report all the load-displacement responses for the tested configurations. In each plot, the monotonic curves are also superposed in order to provide a comparison between the cyclic and monotonic responses.

The results of the two cyclic tests carried out on configuration SS1 showed a good match with the monotonic test, both in terms of load-displacement curves and damage (Figure 3a and 3b). The maximum compressive and tensile loads are equal to 16.1 kN and 18.9 kN, respectively for the first cyclic test. The corresponding maximum compressive and tensile loads are 12.9 kN and 19.0 kN, respectively for the second cyclic test. The maximum displacements achieved during the first test are equal to 63 mm in compression and 78 mm in tension. The corresponding displacement values are 53 mm in compression and 61 mm in tension for the second test. As for the monotonic test, the first drop in each load-displacement curve is due to the yielding of the hinge connecting the diagonal and vertical channels, while the second drop is due to the disconnection of the diagonal channel (Figure 4a). When both diagonal channels disconnected from the vertical channels, the tests were stopped. Note that the gravity load carrying capacities of the specimens were not compromised by the induced damage. Two cyclic tests were also performed to investigate the hysteretic response of configuration SS2. The two specimens differed in the vertical rods. In the first specimen, the vertical rods included retainers while in the second specimen the retainers were not included. The load-displacement responses of the two SS2 specimens are shown in Figures 3c and 3d. In both cases, a good match was observed with the results of the monotonic test. For the first SS2 specimen, the maximum load in compression was equal to 14.2 kN, while a maximum load equal to 12.7 kN was reached in tension. The maximum compressive and tensile loads reached in the second test were equal to 11.4 kN and 10.4 kN, respectively. The maximum displacement achieved during the two cyclic tests was equal to 76 mm both in compression and in tension. Similar to the monotonic test, the deformation of the diagonal rods in the cyclic test became evident already at a displacement of only 5 mm. The presence of the retainers in the vertical rods of the first SS2 specimen caused them to deform in double curvature. Both cyclic tests were stopped at a displacement equal to 76 mm due to the significant deformation of the specimens both in plane and out-of-plane (Figure 4b). As for configuration SS1, the specimens were still able to maintain their gravity load carrying capacity at the end of the tests.

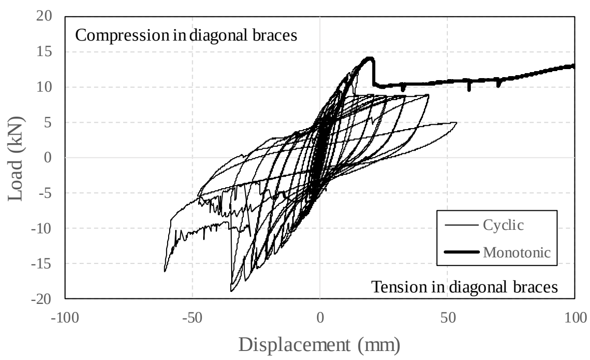

a)

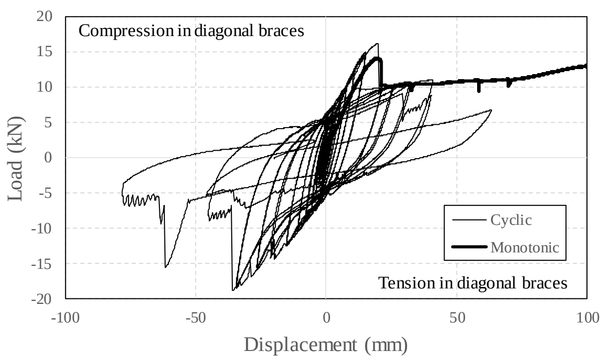

b)

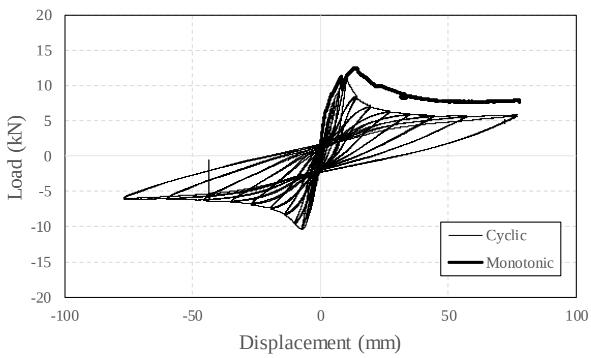

c)

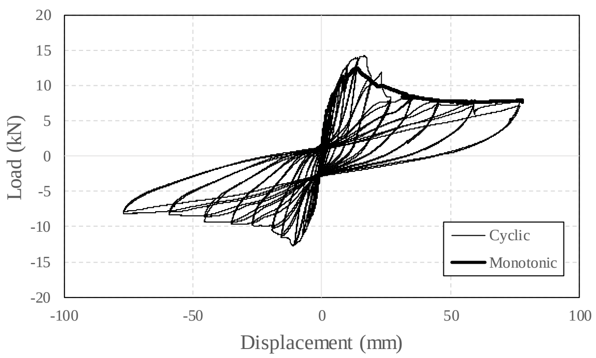

d)

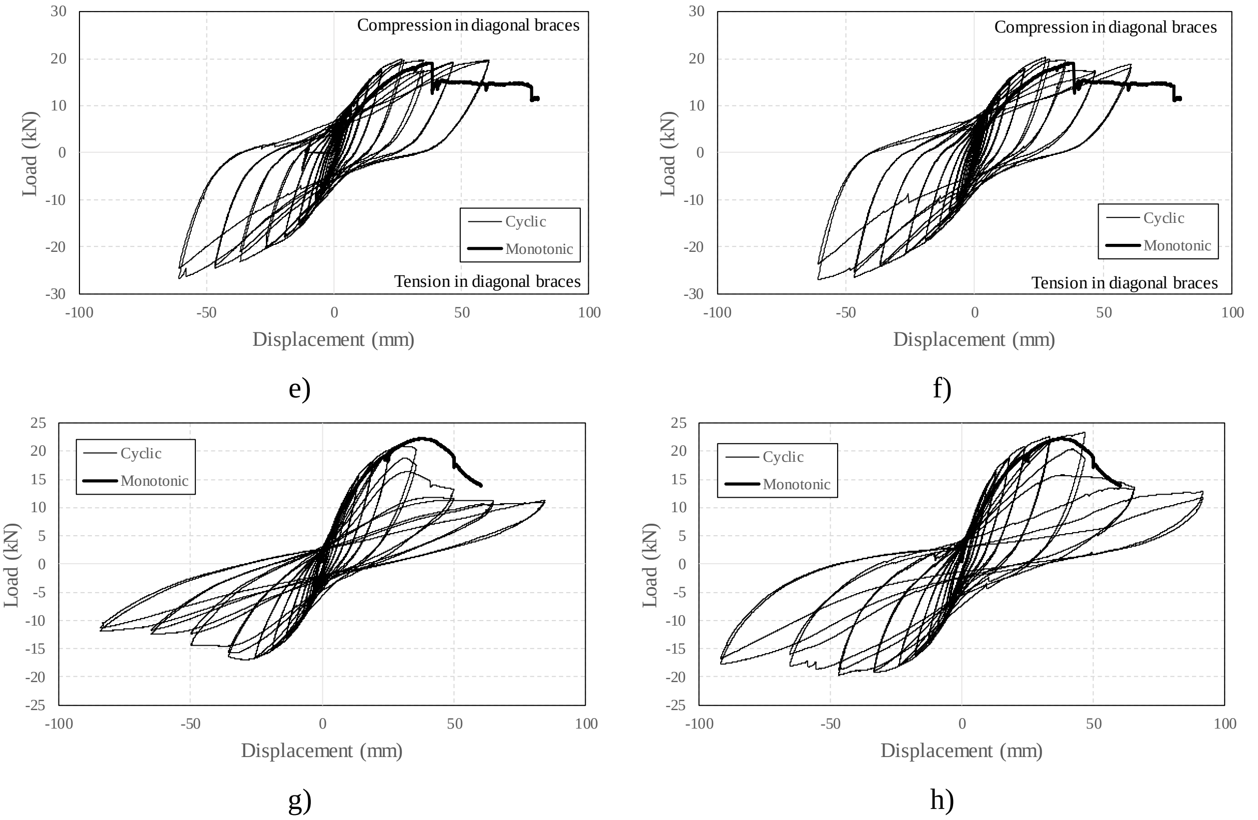

Fig. 3 - Experimental cyclic load-displacement response: a) configuration SS1 first specimen, b) configuration SS1 second specimen, c) configuration SS2 first specimen, d) configuration SS2 second specimen, e) configuration SS3 first specimen, f) configuration SS3 second specimen, g) configuration SS4 first specimen, h) configuration SS4 second specimen

The hysteretic responses of configuration SS3 are shown in Figures 3e and 3f. Also in this case, a good match between the monotonic and cyclic test results is observed. Comparing the maximum load capacities in tension and compression, a higher compression load capacity was achieved. In particular, the maximum load in compression is approximately equal to 20.0 kN, while the load in tension is approximately equal to 27.0 kN, which represents a difference of 34% between compressive and tensile capacities. The maximum displacement achieved during the two tests is equal to 61 mm both in compression and tension. During both cyclic tests, a significant rotation of the specimen around the vertical axis was observed starting from a displacement equal to 36 mm. Both cyclic tests concluded with the shear failure in one of the threaded rods connecting a pipe ring to the horizontal channel (Figure 4c). Flexural and torsional yielding of the horizontal channel was also observed in both specimens. Finally, two cyclic tests were performed to investigate the hysteretic response of configuration SS4 (Figure 3g and 3h). The maximum compressive and tensile loads are equal to 23.3 kN and 19.6 kN, respectively for the first cyclic test. The corresponding maximum compressive and tensile loads are 21.0 kN and 17.0 kN, respectively for the second specimen. As for the other rod configurations, the buckling of the diagonal rods started at small displacements (10 mm). Due to the buckling of both diagonal and vertical rods, a rotation of the specimen around the vertical axis was observed. High torsional deformations of the horizontal channels were also observed near the connection with the vertical and diagonal rods. The tests were stopped at a displacement equal to 92 mm due to the reduction of the horizontal load capacity as well as to the significant deformation of the diagonal and vertical rods (Figure 4d). As for the other three tested configurations, both specimens maintained their gravity load carrying capacity at the end of the tests.

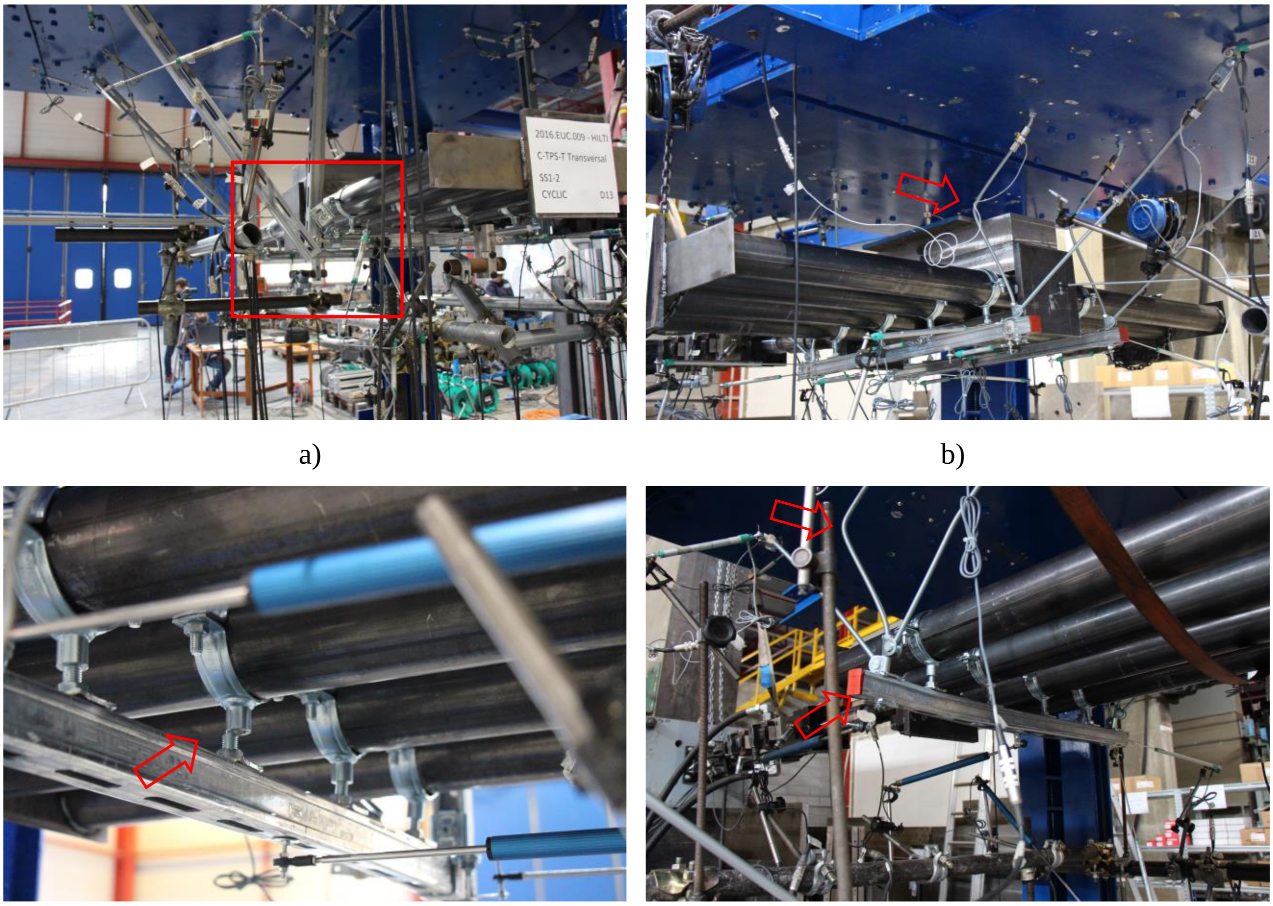

a) b) c) d)

Fig. 4 – Damage observed during cyclic tests: a) configuration SS1: disconnection of the diagonal channel, b) configuration SS2: deformation of the vertical and diagonal rods, c) configuration SS3. Failure of the threaded rod, d) configuration SS4: deformation of the vertical and diagonal rods as well as torsion of the horizontal channel.

4. Numerical modelling

The seismic response of suspended piping systems under building floor motions shaking can be predicted thought advanced nonlinear numerical models. The damage observed during past earthquakes pointed out that the weakest elements of suspended piping systems are the piping joints and the piping restraint installations. Based on this consideration, the numerical modelling of piping systems should account for the nonlinear response of piping joints and restraint installations. While the pipes' behaviour can be simulated through elastic beam elements. The hysteretic moment-rotation capacity at the connection between multiple pipelines can be modelled adopting zero-length bi-directional flexural springs, while the suspended piping restraint installations can be simulated through non-linear shear springs. The dynamic response of piping joints, mainly adopted in fire sprinkler piping systems and medical gas pipelines, was recently investigated both from an experimental and numerical point of view [7,8,10,11]. To the authors' knowledge, no numerical modelling of suspended piping trapeze restraint installations, both at the component and system levels has been reported in the public literature. To fill this gap, Perrone *et al.* [16] developed advanced numerical models of suspended piping trapeze restraint installations based on component testing. Reliable numerical models capable of predicting the force-displacement (backbone) curves of suspended piping trapeze restraint installations was developed based on monotonic and cyclic test data of the components that make up these installations. Although this approach provides accurate numerical models that could be used to predict the force-displacement curves of different suspended piping trapeze restraint installations avoiding to conduct additional sub-assembly testing, it is generally not suitable for the analysis of the seismic response of full scale piping layout. To this aim, simplified numerical models have been developed in this study using the results of the subassembly cyclic tests presented in Section 3. The Pinching4 material model implemented in the OpenSees finite element simulation program [17] was used to model the hysteretic cyclic behaviour of the tested suspended piping trapeze restraint installations. This material model consists of a piecewise linear backbone curve, a piecewise linear unload-reload path, and three damage rules that control the evolution of these paths [18]. Figure 5 reports a general plot of the Pinching4 model illustrating the physical meaning of each parameter that should be calibrated.

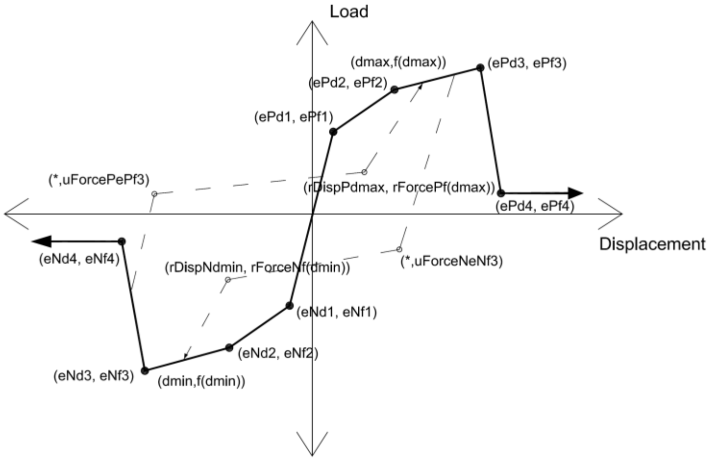

Fig. 5 – Main parameters required to calibrate the Pinching4 model

The Pinching4 material model was selected to fit a mathematical model to the piping restraint trapeze installations because of its versatility. The model can capture both pinching and non-pinching behaviours and it allows for an asymmetrical backbone curve. Figure 6 reports the comparison between the cyclic response obtained during the first cyclic test of each suspended piping restraint trapeze installation and the cyclic behaviour assigned to the nonlinear shear springs using the Pinching4 material. A good match between the experimental results and the numerical predictions is obtained for all configurations. These results demonstrate the effectiveness of using the proposed approach in order to simulate the response of the piping restraint trapeze installations in the dynamic analysis of suspended piping systems. Table 3 reports all the mean parameters, obtained considering the two cyclic tests, required to model the Pinching4 material for the four Suspended trapeze restraint installations tested in this study. All the parameters were obtained by a trial and error procedure and by comparing the experimental and numerically predicted energy dissipated at each cycle.

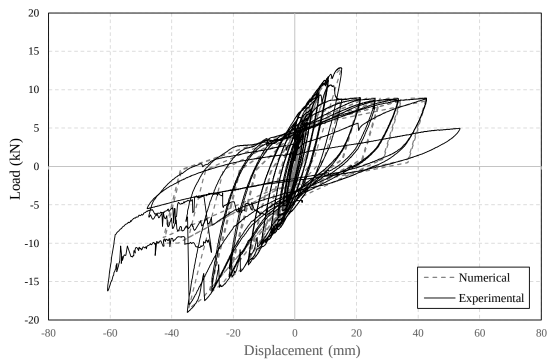

a)

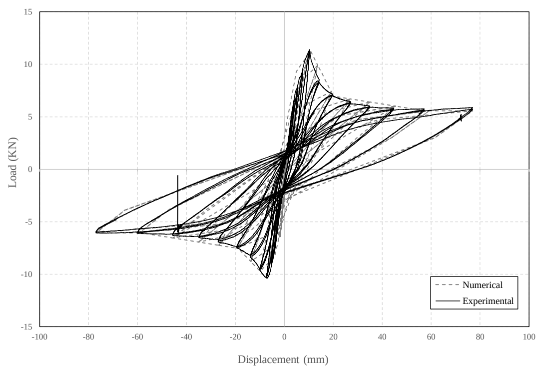

b)

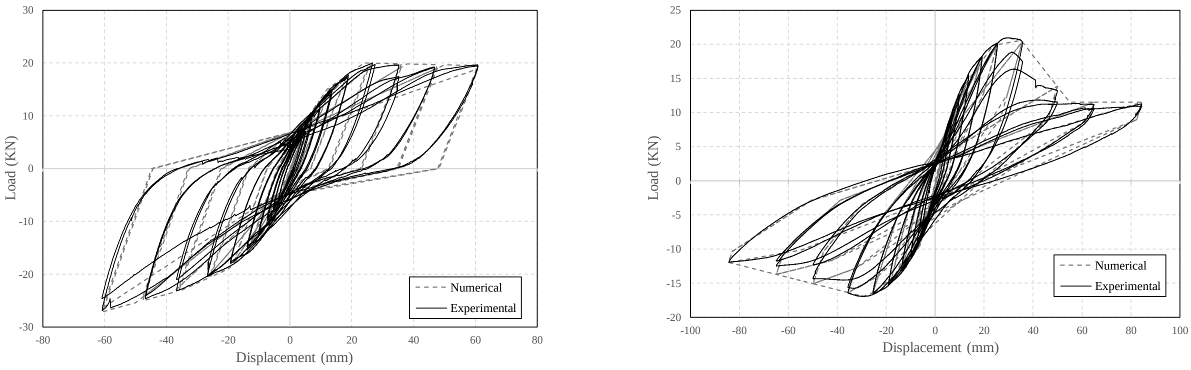

c) d)

Fig. 6 – Comparison between Numerical vs Experimental cyclic load-displacement responses: a) configuration SS1, b) configuration SS2, c) configuration SS3, d) configuration SS4

Table 3 – Pinching4 Material Model Parameters for Tested Suspended Trapeze Restraint installations.

	ePf1 [kN]	**ePf2 [kN]**	**ePf3 [kN]**	**ePf4 [kN]**	**ePd1 [mm]**	**ePd2 [mm]**	**ePd3 [mm]**	**ePd4[mm]**
SS1	5.0	9.0	12.8	8.9	1.5	5.0	15.2	15.2
SS2	6.1	11.4	6.9	5.6	3.67	10.4	20.15	57.7
SS3	10.0	15.0	20.0	19.5	6.0	12.0	24.0	61.0
SS4	12.7	19.8	20.6	11.5	9.5	23.6	35.1	55.0
	eNf1 [kN]	**eNf2 [kN]**	**eNf3 [kN]**	**eNf4 [kN]**	**eNd1 [mm]**	**eNd2 [mm]**	**eNd3 [mm]**	**eNd4 [mm]**
SS1	6.0	13.0	19..0	10.0	1.5	16.0	36.0	36.0
SS2	7,5	10,3	7,5	6,1	4,1	7.3	18.9	58.8
SS3	11.0	19.0	23.0	27.0	6.0	20.0	35.0	60.0
SS4	11.1	15.6	16.9	11.9	9.5	20.1	29.3	84.6
	rDP	**rFP**	**uFP**	**rDN**	**rFN**	**uFN**	**gK1**	**gK2**
SS1	0.1	0.6	-0.05	0.15	0.3	-0.05	0.7	0.0
SS2	0.5	0.85	-0.7	0.4	0.85	-0.5	0.4	0.3
SS3	0.1	0.4	0.0	0.1	0.2	0.0	0.7	0.0
SS4	-0.6	-0.25	-0.9	0.65	0.85	-0.75	0.02	0.03
	gK3	**gK4**	**gKL**	**gD1**	**gD2**	**gD3**	**gD4**	**gDL**
SS1	0.0	0.6	0.6	0.7	0.0	0.0	0.6	0.1
SS2	0.3	0.2	0.9	0.0	0.0	0.0	0.0	0.0
SS3	0.0	0.6	0.1	0.7	0.0	0.0	0.6	0.05
SS4	0.1	0.1	0.1	0.0	0.0	0.0	0.0	0.0
	gF1	**gF2**	**gF3**	**gF4**	**gFL**	**gE**	**dmgType**	
SS1	0.0	0.0	0.0	0.0	0.0	10.0	cycle	
SS2	0.0	0.0	0.0	0.0	0.0	10.0	cycle	
SS3	0.0	0.0	0.0	0.0	0.0	10.0	cycle	
SS4	0.0	0.0	0.0	0.0	0.0	10.0	cycle	

5. Conclusions

The results of monotonic and cyclic tests as well as of the simplified numerical modelling of suspended piping restraint trapeze installations were described in this paper. Four typologies of suspended piping restraint installations were modelled: (1) trapezes with transverse channel bracing systems, (2) trapezes with transverse rod bracing systems, (3) trapezes with longitudinal channel bracing systems, and (4) trapezes with longitudinal rod bracing systems. All suspended piping restraints exhibited a significant strength capacity varying from 14.1 kN to 23.7 kN for the channel trapezes and from 12.5 kN to 22.2 kN for the rod trapezes. No brittle failure occurred in any of the tests and the gravity load carrying capacity was maintained at the end of all tests. For the channel trapezes, the deformations were mainly concentrated in the components connecting the channel elements. For the rod trapezes, significant deformations and buckling of the rods were observed. The results of the cyclic tests were used to develop simplified numerical models represented by zero-length shear springs. The Pinching4 material available in OpenSees was used to calibrate the numerical models. The good match between the numerical calibration and the experimental results demonstrated the effectiveness of using this simplified numerical modelling approach for the seismic performance assessment of suspended piping systems.

6. Acknowledgements

The experimental program and the numerical modelling described in this paper was conducted as part of a collaborative research program between Hilti Corporation and the European Centre for Training and Research in Earthquake Engineering (EUCENTRE) Foundation. The work has been also developed within the framework of the project "Dipartimenti di Eccellenza", funded by the Italian Ministry of University and Research at the University School for Advanced Studies IUSS Pavia.

7. References

[1] Perrone D, Calvi PM, Nascimbene R, Fischer E, Magliulo G (2018): Seismic performance and damage observation of non-structural elements during the 2016 Central Italy Earthquake. *Bulletin of Earthquake Engineering*, DOI: 10.1007/s10518-018-0361-5.

[2] Ercolino M, Petrone C, Coppola O, Magliulo G (2012): *Report sui danni registrati a San Felice sul Panaro (Mo) in seguito agli eventi sismici del 20 e 29 maggio 2012* – v1.0. available on line: http://www.reluis.it.

[3] Filiatrault A, Uang CM, Folz B, Christopoulos C, Gatto K (2001): Reconnaissance report of the February 28, 2001 Nisqually (Seattle-Olympia) earthquake. *Structural Systems Research Project Report No. SSRP-2000/15*, Department of Structural Engineering, University of California, San Diego, La Jolla, CA, 62 pp.

[4] Chock G, Robertson I, Nicholson P, Brandes H, Medley E, Okubo P, Hirshorn B, Sumada J, Kindred T, Linurna G, Sarwar A, Dal Pino J and Holme W. (2006): Compilation of observations of the October 15, 2006, Kiholo Bay (Mw 6.7) and Mahukona (Mw 6.0) earthquakes, Hawaii. *Earthquake Engineering Research Institute*, Oakland, California, 53 pp.

[5] Miranda E, Mosqueda G, Retamales G, Pekcan G (2012): Performance of nonstructural components during the 27 February 2010 Chile earthquake. *Earthquake Spectra,* 28(S1):S453–S471.

[6] Miranda E, Taghavi, S (2003): Estimation of seismic demands on acceleration-sensitive non-structural components in critical Facilities. *Seminar on Seismic Design, Performance, and Retrofit of Non-structural Components in Critical Facilities*, ATC 29–2, Newport Beach, California, 347–360.

[7] Tian Y, Filiatrault A, Mosqueda G (2015): Seismic response of pressurized fire sprinkler piping systems I: experimental study. *Journal of Earthquake Engineering*, 19(4):649–673.

[8] Blasi G, Aiello MA, Maddaloni G, Pecce MR (2018): Seismic response evaluation of medical gas and fire-protection pipelines' Tee-Joints. *Engineering Structures*, 173, 1039–1053.

[9] Filiatrault A, Perrone D, Merino RJ, Calvi GM (2018): Performance-based seismic design of non-structural building elements. *Journal of Earthquake Engineering,* DOI: 10.1080/13632469.2018.1512910.

[10] Tian Y, Filiatrault A, Mosqueda G. (2015): Seismic response of pressurized fire sprinkler piping systems II: Numerical study. *Journal of Earthquake Engineering*, 19(4), 674–699.

[11] Soroushian S, Zaghi AE, Maragakis EM, Echevarria A, Tian Y, Filiatrault A (2015): Seismic Fragility Study of Fire Sprinkler Piping Systems with Grooved Fit Joints. *Journal of Structural Engineering*, 141(6), 04014157.

[12] Wood RL, Hutchinson TC, Hoehler MS, Kreidl B (2014): Experimental characterization of trapeze assemblies supporting suspended non-structural systems. *Proc. of the Tenth U.S. National Conference on Earthquake Engineering*, Paper No. 905, Anchorage, Alaska, 10 p.

[13] Perrone D, Filiatrault A, Peloso S, Brunesi E, Beiter C, Piccinin R (2019): Experimental seismic performance evaluation of suspended piping restraint installations. *Bulletin of Earthquake Engineering*, DOI 10.1007/s10518-019-00755-5.

[14] Hilti (2014): Earthquake resistant design of installations, *Ed 1.1*, Schaan, Liechtenstein, 104 pp.

[15] FEMA (2007): FEMA 461: Interim testing protocols for determining the seismic performance characteristics of structural and nonstructural components. *Federal Emergency Management Agency*, Washington, D.C.

[16] Perrone D, Brunesi E, Filiatrault A, Peloso S, Nascimbene R, Beiter C, Piccinin R (2020): Seismic Numerical Modelling of Suspended Piping Trapeze Restraint Installations Based on Component Testing. *Bulletin of Earthquake Engineering*, Under Review.

[17] Mazzoni S, McKenna F, Scott MH, Fenves GL (2006): *OpenSees Command language manual*. Pacific Earthquake Engineering Research Center, Berkeley, California.

[18] Lowes LN, Mitra N, Altoontash A (2004): A beam-column joint model for simulating the earthquake response of reinforced concrete frames. *PEER Report 2003/10*. Pacific Earthquake Engineering Research Center, University of California Berkeley, USA.

